

Microstructure and Mechanical Properties of Plasma Arc Welded Joints Made of Austenitic Steel

Abstract: The tests discussed in the article aimed to analyse the microstructure and properties of plasma arc-welded joints (process 15) used in tests concerning welding procedure approval. The material subjected to the tests was austenitic steel X5CrNi18-10, belonging to a group of structural materials characterised by special properties (high corrosion resistance, favourable mechanical properties and good weldability). Because of its advantages, the steel is used in many industrial sectors and joined using various welding techniques. The article presents results obtained using the plasma arc welding process (PAW), which, due to its advantages, enjoys growing popularity in many industries. The test joints were subjected to macro and microscopic metallographic tests, mechanical tests (tensile tests, bend tests and hardness measurements) and diffraction tests.

Keywords: austenitic steel, plasma arc welding (PAW), microstructure, mechanical testing

DOI: 10.17729/ebis.2023.4/5

Introduction

Because of their favourable corrosion resistance in aggressive environments, stainless steels are rated among structural materials of special properties [1-4]. Basically, within the entire range of temperatures, stainless steels contain one phase, i.e. austenite. Depending on the chemical composition of a given steel grade, it is also possible to observe a slight fraction of high-chromium ferrite δ (approximately 10%) [5, 6]. The presence of austenite is responsible for an increase in the yield point and tensile strength [5, 7, 8].

Austenitic steels are characterised by high ductility, elasticity, formability [4] and crack resistance at cryogenic temperatures [1]. The applicability of such steel at the above-named temperatures results from the lack of transition to the brittle state [1, 2]. Classical austenitic steels are characterised by good weldability enabling the attainment of appropriate strength, corrosion resistance, toughness and ductility in the weld and heat affected zone (HAZ). The aforesaid advantages result, among other things, from the fact that the formation of undesired phases in the structure requires

longer exposure to high temperature (entailing lower cooling rates) than that during the welding thermal cycle. Because austenitic steels do not undergo hardening during fast cooling, the heat affected zone does not contain hardening structure and is not characterised by grain growth [9, 10].

Stainless steels can be welded using several methods. The selection of a proper method depends on a given type of alloy. An improperly selected welding method could negatively affect the material structure.

The plasma arc welding (PAW) of stainless steels is not so commonly used in industry as TIG (process 141 in accordance with EN 4063) and MIG methods (process 131 in accordance with EN 4063) [11]. The advantages of the PAW process include higher welding rates (because of higher energy concentration, stability and plasma beam adjustability) and the possibility of welding thick plates using relatively narrow runs with significant penetration depths (translating into lower stresses and strains) [12, 13]. The development of the technique is responsible for the fact that the PAW method is enjoying continuous applicability in relation

to elements characterised by the highest requirements concerning the quality of the weld (lack of spatter and porosity as well as very high aesthetics). Increasingly often it is possible to come across PAW equipment and welding stations used for the joining of vessels and other products made of stainless steels having thicknesses restricted within the range of 6 mm to 8 mm (or even thicker). The PAW process constitutes an alternative to TIG or MIG welding methods.

The article discusses results obtained in tests concerning plasma arc welded joints (process 15) and accompanying the process of welding procedure approval. The process of welding procedure approval was performed in accordance with the requirements specified in the PN-EN ISO 15613 standard [14], including the performance of an additional test, i.e. the observation of microstructure in the joint area. The material subjected to welding was 8 mm thick steel X5CrNi18-10 (AISI 304).

Test materials and methodology

The subject of the tests discussed in the article was an 8 mm thick butt welded joint made of steel X5CrNi18-10 (having the form of flat bars) using the PAW method (process 15 in accordance with ISO 4063 [15]). The chemical composition of the test steel is presented in Table 1.

Figure 1 presents the structure of the base material, i.e. the classical microstructure obtained in hot-rolled austenitic steels. It is possible to observe annealing microtwins. The visible banded

structure resulted from the plastic treatment of the plates. It was also possible to notice some darker areas of ferrite.

The tests of the welded joints included (macro and microscopic) metallographic tests, mechanical tests (static tensile test, static bend test and hardness measurements) and diffraction tests.

The microstructural observations of the welded joints were performed using a DMLM 4000M light microscope (Leica). The metallographic specimens used in the tests were previously subjected to electrolytic etching. The etching process was performed at room temperature and involved the use of a voltage of 6 V and etching time restricted within the range of 10 s to 40 s. The etchant contained 10 g of oxalic acid and 100 ml of H₂O. Such an approach made it possible to reveal the fusion line and the heat affected zone (HAZ). Microstructural observations included the weld, the heat affected zone (HAZ) and the base material. The metallographic tests were preceded by macroscopic observations performed using a stereoscopic microscope.

The static tensile test was performed in accordance with the requirements specified in the PN-EN ISO 6892-1:2016-09 standard [17], using an MTS 810 testing machine. The specimens subjected to the tests were sampled perpendicularly to the weld axis. The test involved rectangular specimens (7 mm × 7 mm), maintaining the length of measurement part $L_0 = 72$ mm. The weld face and root were subjected to mechanical treatment. The

Table 1. Chemical composition of steel X5CrNi18-10 in accordance with PN-EN 10088-2: 2014-12 [16]

Steel grade	C	Si	Mn	P	S	Cr	Ni
X5CrNi18-10	<0.05	<0.75	<2.0	<0.04	<0.015	17.5–19.0	8.0–10.0



Fig. 1. Microstructure of the base material, i.e. steel X5CrNi18-10

cross-beam travel rate amounted to 10 mm/min. The tensile tests involved the use of 3 specimens.

The static three-point side bend test was performed in accordance with the recommendations specified in the PN-EN ISO 5173:2010 standard [18] and involved the use of non-standard specimens having dimensions of 100 mm × 6 mm × 8 mm. The specimens were cut out perpendicularly to the weld axis. In order to remove the reinforcement and collar of the weld root, the specimens were subjected to mechanical treatment. The test was performed using a bending pin having a diameter of 32 mm, i.e. being four-fold thicker than the base material. The bend test involved the material of the weld.

The hardness measurements were performed in accordance with the requirements specified in the PN-EN ISO 9015:2011 standard [19] and involved the use of a Zwick/Roell ZHU 187.5 universal hardness tester. The measurements involved the use of the Vickers hardness test, performed in accordance with the requirements specified in the PN-EN ISO 6507:2007 [20], and a load of 49 N (HV5). The specimens used in the tests were sampled perpendicularly to the weld axis and contained the centrally located cross-section of the welded joint, indispensable for the proper arrangement of measurement points.

In each specimen, indents were made in two measurement lines (rows (R)) crossing the base material, HAZ and the weld. Both lines were located 2 mm away from the plate surface. Because of the very narrow area of the heat affected zone (HAZ), hardness measurements in the zone were performed on the measurement line and, in addition, above and below it.

The radiographic tests involved the use of a D8 Advance (Bruker) diffractometer equipped

with an X-ray tube featuring cobalt anode $\lambda_{Co} = 0.17902$ nm. The measurement conditions included angle range $2\theta = 45^\circ - 125^\circ$, measurement increment $\Delta 2\theta = 0.04^\circ$ and time $\tau = 10$ s/increment.

Test results

The results of the macroscopic metallographic tests are presented in Figure 2, whereas the results of the microscopic tests are presented in Figures 3 through 5. The two-run weld was characterised by a relatively large face width of ~11.5 mm and symmetry in relation to the weld axis. Both the dimensions of the weld face and those of the weld root were restricted within the range of boundary values concerning imperfection dimensions in relation to quality level B in accordance with the PN-EN ISO 5817 standard [21]. The observations did not reveal the presence of any other internal welding imperfections such as cracks, incomplete fusion or porosity. It was possible to observe that individual dendrites grew in both layers, which indicated the occurrence of the so-called transcrystallisation. In addition, dendrites were also observed in the central area of the weld, which is characteristic of the crystallisation of welds made of austenitic steels. A darker area observed near the fusion line in the macrostructural photograph was the heat affected zone.

Figure 3 presents the microstructure of the weld made of steel X5CrNi18-10, composed of the austenitic matrix and precipitates of ferrite (lamellar and reticular). Figure 4 presents the weld microstructure in the fusion line with the weld and the heat affected zone, whereas Figure 5 presents the central area of the weld. The structure of steel X5CrNi18-10 was purely austenitic. The ferritic nature of steel crystallisation combined with

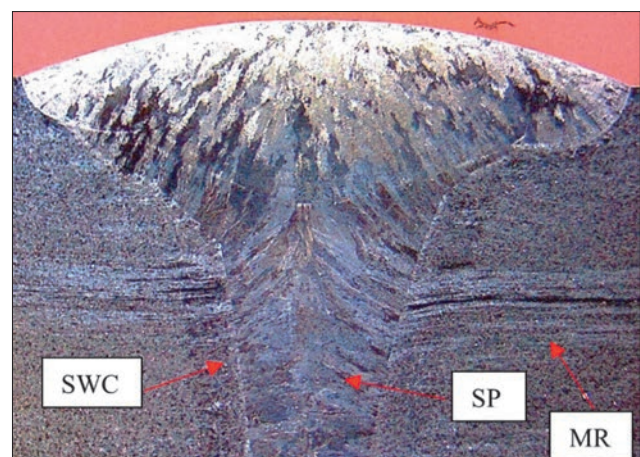


Fig. 2. Macrostructure of the welded joint made of steel X5CrNi18-10

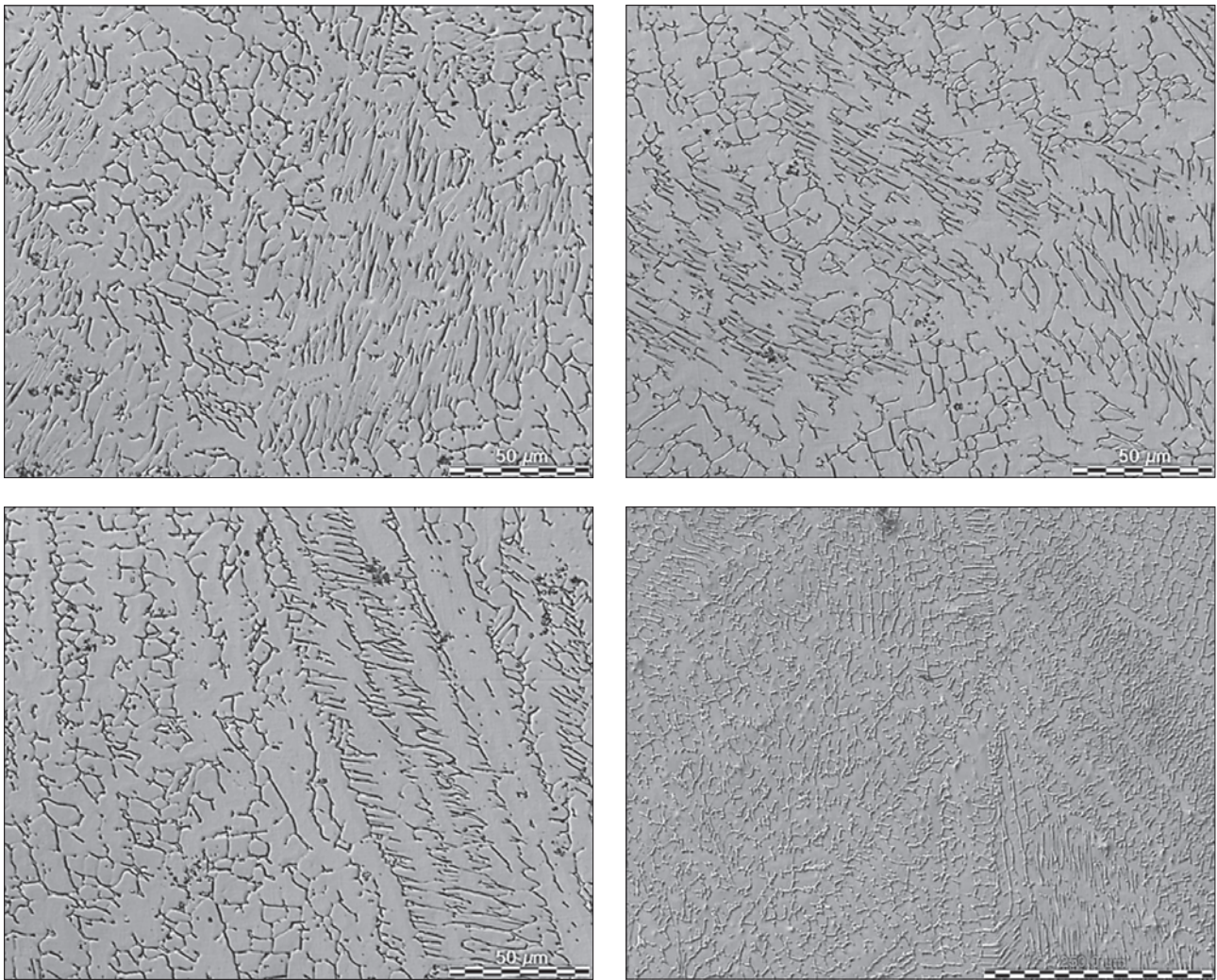


Fig. 3. Weld microstructure

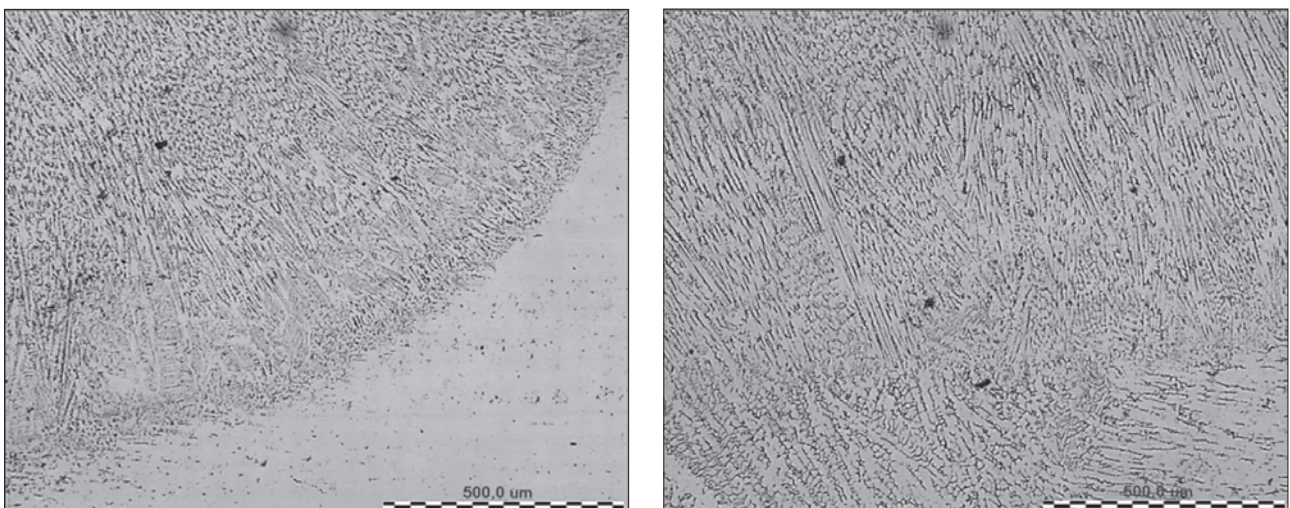


Fig. 4. Microstructure in the fusion line area

post-weld segregation processes were responsible for the fact that the structure of the welds made of steel X5CrNi18-10 was composed of austenite and a certain amount of ferrite. During the crystallisation from the liquid state the nature of phase transformations changed $L \rightarrow L + \delta \rightarrow \delta \rightarrow \delta +$

$\gamma \rightarrow \gamma$ [9]. In terms of welding, the cooling process was so fast that crystallisation was of non-equilibrium nature and, up to ambient temperature, the weld structure contained a certain amount of ferrite δ . The faster the cooling above a temperature of 1250°C, the greater the amount of ferrite.

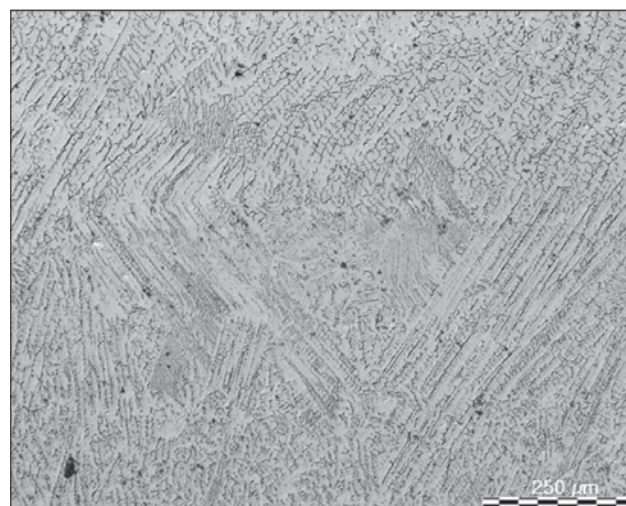
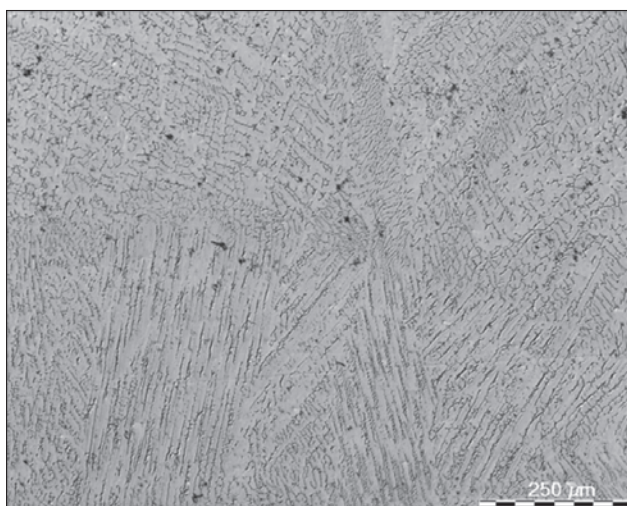


Fig. 5. Microstructure in the fusion line area between the runs

The formation of the above-named phase was also significantly affected by segregation taking place during crystallisation. The aforesaid segregation increased the life of the structure and reduced the rate of ferrite transformation into austenite [9].

Figure 6 presents the diagram of the static tensile test. The material did not reveal a clearly noticeable yield point. During the test it was possible to observe a plastic strain in the form of a neck (see Fig. 7) located in the weld. The tests of the weld made of steel X5CrNi18-10 revealed conventional yield point $R_{p0.2} = 321.9$ MPa, tensile strength $R_m = 547.7$ MPa and relative elongation $A = 52.5\%$, whereas the mechanical properties of steel X5CrNi18-10 in accordance with PN-EN 10088-2: 2014-12 [16] included $R_{p0.2\min} = 210$ MPa, $R_m = 520-720$ MPa and $A_{\min} = 45\%$ (Table 2). As can be seen, the joint was characterised by higher yield point than the value required in relation to steel X5CrNi18-10 not subjected to welding. The test result satisfied the requirement specified, among other things, in the PN-EN ISO 15614-1 standard [22], according to which the tensile

strength of the specimen should be not lower than the specified lowest tensile strength of the base material.

Table 2. Results obtained in the static tensile test

	Joint	Steel X5CrNi18-10 in accordance with PN-EN 10088-2: 2014-12 [16]
$R_{p0.2}$ [MPa]	321.9	>210
R_m [MPa]	547.7	520–720
A [%]	52.5	>45



Fig. 7. Specimen after the static tensile test

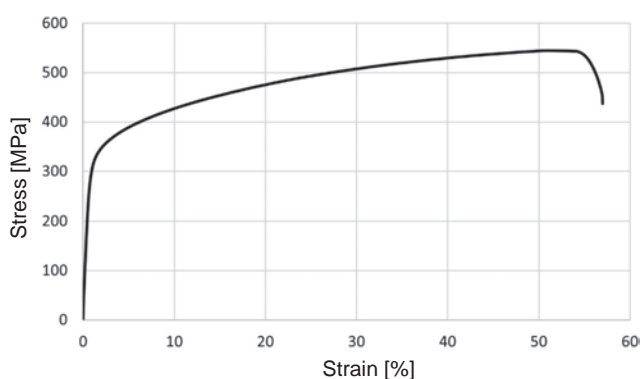


Fig. 6. Stress-strain curve concerning the welded joint made of steel X5CrNi18-10

The three-point bend test involved the use of a bending pin. A bend angle of 160° obtained without cracks or partial tear confirmed high plastic properties of the welded joint. The maximum strength preceding the bending of the specimen amounted 3550 N.

Figure 8 presents the specimen after the bend test.

The Vickers test-based hardness measurements were performed in two lines, i.e. on the weld face and weld root side (Fig. 9). The tests revealed a slight increase in hardness in the HAZ and in the weld (on the weld root side) in comparison with that of the base material as well as revealed a slight decrease in hardness in the HAZ and in the weld (on the weld face side) in comparison with the hardness of the base material. The lowest hardness of 164 HV5 was measured on the weld face side, whereas the highest hardness of 260 HV5

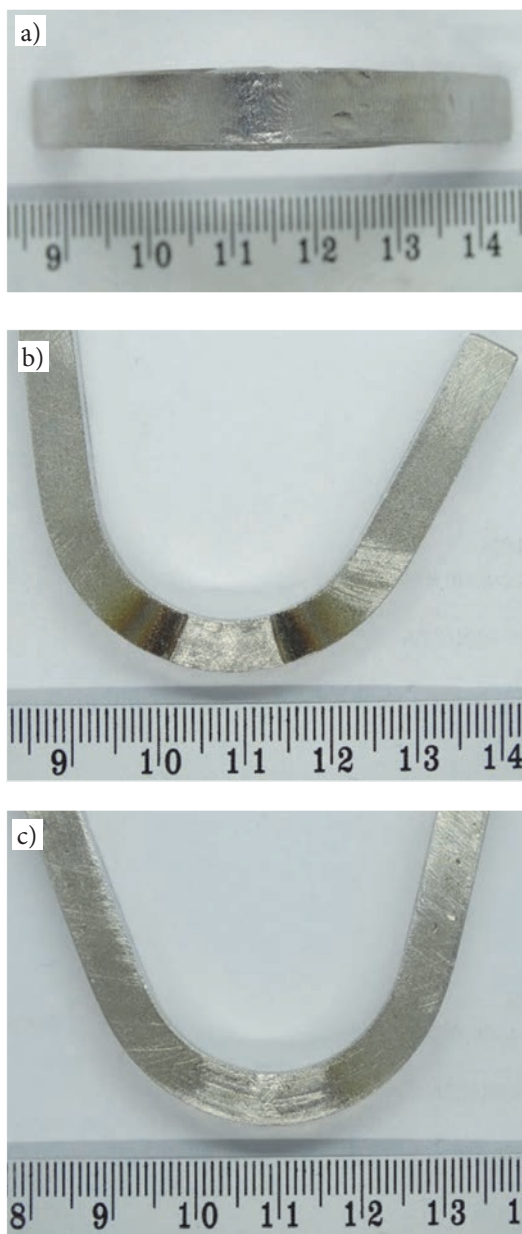


Fig. 8. Specimen after the three-point side bend test: a) bend side view, b) view from the weld face, c) view from the weld root

was measured on the weld root side. The X-ray phase analysis and the analysis of diffraction lines made it possible to analyse the phase composition and changes (if any) in the weld in relation to the base material.

Figure 10a presents the diffraction record of the base material, whereas Figure 10b presents the record obtained in relation to the weld. In both diffraction patterns it was possible to observe strong peaks originating from austenite and weak peaks originating from ferrite. The strongest peak observed in the base material was $(111)\gamma$. It was also possible to observe a strong line originating from $(200)\gamma$ and weaker lines originating from $(311)\gamma$, $(220)\gamma$ and $(222)\gamma$. In addition, it was possible to observe a weak peak originating from ferrite $(110)\alpha$. In the weld, the strongest line was that originating from $(111)\gamma$. It was also possible to observe a strong peak originating from $(200)\gamma$. The intensity of both lines was significantly higher in the weld than in the base material. In turn, it was possible to observe the weakening of the peak originating from $(311)\gamma$. It was also possible to observe an increase in the intensity of line $(110)\alpha$ and the appearance of an additional (yet weak) peak originating from ferrite $(200)\alpha$. The test involved the calculation of the reflection intensity ratio for austenite $I_{\gamma111}/I_{\gamma200}$ and $I_{\gamma111}/I_{\gamma220}$ as well as for ferrite $I_{\alpha110}/I_{\alpha200}$ and the comparison of the above-named values with theoretical values for the PDF standard specimen from the ICDD base. The analysis of the aforementioned simple indicators enabled the detection of the presence and strength of the crystallographic texture.

The results of the test are presented in Table 3. The differences between theoretical values and

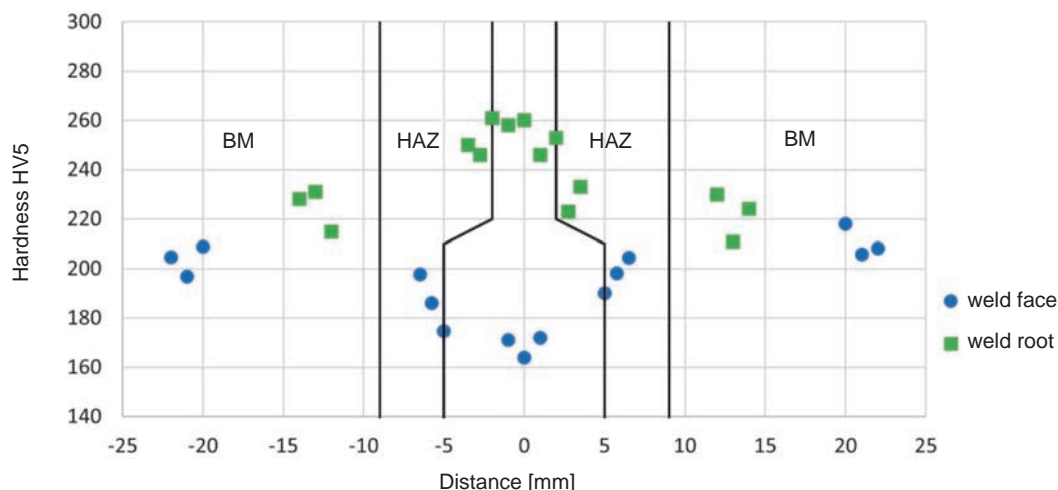


Fig. 9. Hardness distribution in the weld, heat affected zone (HAZ) and in the base material (BM), measured in cross-section, on the side of the weld face and weld root

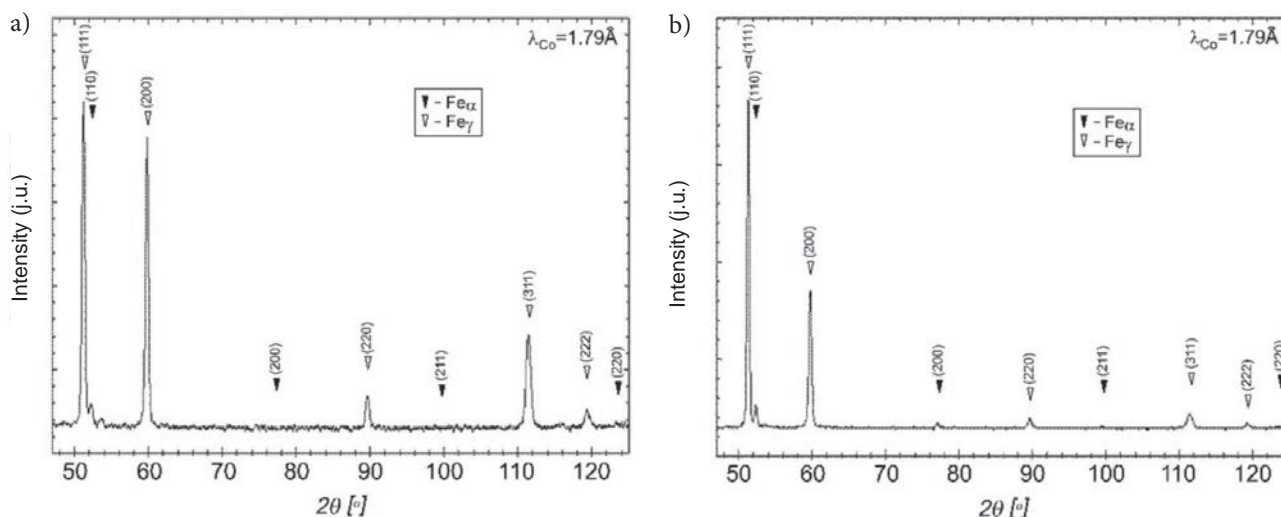


Fig. 10. Diffraction patterns of the base material (steel X5CrNi18-10) (a) and weld (b)

experimentally identified intensity ratios indicated the texturisation of the material.

Table 3. Austenite and ferrite peak intensity ratios for steel X5CrNi18-10 subjected to plasma arc welding

Material	$I_{\gamma111}/I_{\gamma200}$	$I_{\gamma111}/I_{\gamma220}$	$I_{\alpha110}/I_{\alpha200}$
Theoretical value	2	3.1	5
Base material	1.1	7.8	–
Weld	1.9	23.1	4.8

Conclusions

The microstructure of the weld made of the austenitic chromium-nickel steel was composed of austenite and ferrite of two, i.e. lamellar and reticular, morphologies.

The weld made of steel X5CrNi18-10 using plasma arc welding method was relatively plastic, which was confirmed by the bend test result.

The results of the static tensile test revealed that the material after welding satisfied requirements concerning mechanical properties.

The differences concerning the intensity between the standard specimen and the test material, observed during the diffraction phase analysis, revealed the texturisation of the material.

The study was funded by the Ministry of Science and Higher Education within research subsidy no. 16.16.110.663 for the AGH University of Science and Technology in Kraków.

References

- Jiang W., Zhu K., Li J., Qin W., Zhou J., Li Z., Gui K., Zhao Y., Mao Q., Wang B.: Extraordinary strength and ductility of cold-rolled 304L stainless steel at cryogenic temperature. *Journal of Materials Research and Technology*, 2023, vol. 26, pp. 2001-2008.
- Li J., Cheng W., Qin W., Chen M., Zhao Y., Li Y., Sun Y., Mao Q.: Cryogenic impact property of a high-strength-ductility 304L stainless steel with heterogeneous lamella structure. *Journal of Materials Research and Technology*, 2023, vol. 24, pp. 1401-1409.
- Gupta S.K., Patil A.P., Rathod R.C., Tandon V., Gupta A.: Characterization of microstructure, mechanical and corrosion response in AISI 304L and Ti-stabilized 439 stainless steels weld joints. *Journal of Manufacturing Processes*, 2023, vol. 101, pp. 721-736.
- Jaleel A., Narayanan C.S.: Formability investigation of perforated austenitic SS 304L sheets using SPIF. *Journal of Manufacturing Processes*, 2023, vol. 104, pp. 44.
- Zhao X., He F., Wang K., Lu X.: Investigation on the microstructure and mechanical properties analysis of 304L stainless steel multi-pass filler welding joint for pipeline. *Materials Today Communications*, 2022, vol. 33, 104770.
- Kowalska J., Ratuszek W., Ryś J., Chruściel K.: Analysis of deformation and annealing textures in austenitic steel with ferrite precipitates. *XIX Conference on Applied Crystallography, Kraków 2003*, pp. 190-195.
- Pickering F.B.: *Rozwój metaloznawstwa stali odpornych na korozję*. Hutnik, 1978, no. 8-9, pp. 343-365.
- Lamb S. (ed.): *Casti handbook of stainless steels&nickel alloys*, Casti Pub., Canada 2021.
- Tasak E.: *Metalurgia spawania*, JAK, Kraków 2008.
- Tasak E.: *Spawalność stali*, Fotobit, Kraków 2002.
- Li W., Chen J., Tatman J., Feng Z., Latour M., Miller R., Walters L., Rosseel T.M., Frederick G.: Weldability of irradiated Stainless Steel 304 materials harvested from the National Research Universal (NRU) reactor. *Journal of Nuclear Materials*, 2023, vol. 574, 154193.
- Casanueva R., Branas C., Diaz F.J., Azcondo F.J., Ferreno D., Setien J.: Characterization of an energy efficient pulsed current TIG welding process on AISI 316 and 304 stainless steels. *Heliyon*, 2023, 9, e19819.
- Sajek A., Nowacki J.: Comparative evaluation of various experimental and numerical simulation methods for determination of $t_{8/5}$ cooling times in HPAW process weldments. *Archives of Civil and Mechanical Engineering*, 2018, vol. 18, pp. 583-591.

- [14] PN-EN ISO 15613:2006 – Specyfikacja i kwalifikowanie technologii spawania metali – Kwalifikowanie na podstawie przedprodukcyjnego badania spawania/zgrzewania.
- [15] PN-EN ISO 4063: 2002 - Spawanie i procesy pokrewne – Nazwy i numery procesów.
- [16] PN-EN 10088-2: 2014-12 Definicja i klasyfikacja gatunków stali.
- [17] PN-EN ISO 6892-1: 2016-09 – Metale – Próba rozciągania – Metoda badania w temperaturze pokojowej.
- [18] PN-EN ISO 5173: 2010 – Badania niszczące spoin w materiałach metalowych – Badanie na zginanie.
- [19] PN-EN ISO 9015:2011 – Badania niszczące złączy spawanych metali – Badanie twardości – Część 1: Badanie twardości złączy spawanych łukowo.
- [20] PN-EN ISO 6507:2007 – Metale – Pomiar twardości sposobem Vickersa – Część 1: Metoda badań.
- [21] PN-EN ISO 5817:2023-08 – Spawanie – Złącza spawane ze stali, niklu, tytanu i ich stopów (z wyjątkiem spawanych wiązka) – Poziomy jakości dla niezgodności spawalniczych.
- [22] PN-EN ISO 15614-1:2017 – Specyfikacja i kwalifikowanie technologii spawania metali – Badanie technologii spawania – Część 1: Spawanie łukowe i gazowe stali oraz spawanie łukowe niklu i stopów niklu.